Design and demonstration of Knudsen heat pump without moving parts free from electricity

K. Kugimoto,[1,2,a)] Y. Hirota,[1,b)] T. Yamauchi,[1,c)] H. Yamaguchi,[2,d)] and T. Niimi[2) †]

[1] *Toyota Central R&D Labs., Inc., 41-1 Yokomichi, Nagakute, Aichi 480-1192, Japan*

[2] *Department of Micro-Nano Mechanical Science and Engineering, Nagoya University, Chikusa Furo-cho, Nagoya, Aichi 464-8603, Japan*

† *Deceased 14 October 2018*

A heat pump with low power consumption and a simple mechanical configuration is required to save energy and reduce carbon dioxide emissions. We show the design and demonstration of a novel heat pump using a Knudsen compressor, referring this device as a Knudsen heat pump. Water is employed as a refrigerant. The motionless nature of the Knudsen heat pump is accomplished by using a Knudsen compressor to transport the refrigerant vapor from the evaporator to the condenser, and thermal energy alone supplies the needed power. We employ a simple single-stage Knudsen compressor powered by light from a halogen lamp as an energy source. Experiments confirmed heat transport from the evaporator to the condenser with an output power of 3.09 W. The output power tended to increase linearly as the temperature difference between the evaporator and condenser decreased. The pressure-enthalpy diagram of the proposed Knudsen heat pump cycle was shown, and the thermal efficiency of this heat pump was analyzed. The application of a multi-stage Knudsen compressor to improve the heat pump performance was also discussed. This heat pump is free from noise, vibration, and maintenance, and it can utilize low-quality energy, such as a solar energy, and it does not require any electrical input. These properties make the Knudsen heat pump a particularly significant technology in harsh environments such as space and desert.

a) **kugimoto@mosk.tytlabs.co.jp**

b) **e1476@mosk.tytlabs.co.jp**

c) **t-yamauchi@mosk.tytlabs.co.jp**

d) **hiroki@nagoya-u.jp**

Keywords: thermal molecular pump; micro gaseous flow; high Knudsen number flow; thermal transpiration; heat recovery; low-quality energy

1 Introduction

An air conditioner or refrigerator with a heat pump is one of the most common electric appliances for residential and industrial use [1]. Reducing the electricity consumption of the heat pump is very important for saving energy and reducing

carbon dioxide emissions. As a solution to this problem, a chemical heat pump (CHP) has been proposed [2, 3]. A CHP replaces the electric compressor normally used to transport refrigerant vapor from an evaporator to a condenser with a chemical compressor using absorption or adsorption. Because a chemical compressor can make use of waste or renewable heat, the electrical consumption per unit of output power is lower in a CHP than in a conventional heat pump with an electric compressor. In recent years, a lot of work has been devoted to improving the energy efficiency and output power per unit volume of CHPs [4-7]. However, a CHP requires many switching devices in the flow path powered by electricity, such as on-off and three-way switching valves, because it is not possible to generate a steady gas flow with a chemical compressor. In a practical configuration, a CHP uses two adsorbents (or absorbents), and they alternately remove refrigerant vapor from an evaporator by adsorption and discharge it to a condenser by desorption. The adsorption and desorption can also be carried out by alternately transporting a heating and cooling medium to the two adsorbents. Therefore, in a CHP, it is necessary to switch both of the gas flow paths between the evaporator, condenser, and adsorbents, and to switch the liquid flow paths of the heating and cooling medium. Although these switching devices make it impossible to develop a CHP that needs no electricity, they also impose limits on device size, durability, and maintainability.

To address these issues, we focused on a Knudsen compressor (KC) using thermal transpiration [8], which is a one-way gas flow peculiar to a high-Knudsen-number environment induced by a temperature gradient along a microchannel without any mechanical moving parts. Since Knudsen first observed thermal transpiration at low pressures experimentally [9, 10], many studies have been performed, mainly for academic interest [11-15]. Recently, microporous materials and microfabrication technologies have realized thermal transpiration at relatively high pressures, such as atmospheric pressure [16, 17]. Subsequently, thermal transpiration and KCs have attracted interest for use in micro-scale systems, and several practical applications have been proposed. For example, Liu *et al*. and Qin and Gianchandani proposed and demonstrated a micro-gas chromatography system with a miniature Knudsen pump [18, 19]. Nakaye and Sugimoto investigated a gas separator composed of Knudsen pumps [20]. Pharas and McNamara fabricated a bidirectional Knudsen pump by using a thermoelectric material [21], and Gerdroodbary *et al*. analyzed the thermal transpiration in the MEMS gas sensor and actuator [22-24]. Nonetheless, KC applications are still limited because the output of a KC is too small for it to be a suitable replacement for an electric compressor. However, in recent research, a significant increase in the flow rate of a KC was reported [25], and there is a possibility that KCs can be more widely applied in the future.

Following these developments, we proposed a novel concept for using a KC to realize a heat pump, called a Knudsen heat pump (KHP), which has no switching devices [26, 27]. The KHP is composed of a KC, evaporator, condenser, and capillary tube. Refrigerant vapor is transported from the evaporator to the condenser by the KC, and the liquid refrigerant is

returned from the condenser to the evaporator through the capillary tube by a pressure difference and gravity. The KHP is environmentally friendly because it does not require any electricity, and water can be used as a refrigerant. The feature of operation without moving parts also imparts many advantages, such as durability and freedom from noise, vibration, oil, and maintenance. The KHP can be used not only for saving energy in households and factories but also in remote or harsh environments, such as deserts and space, where maintenance and a stable electrical power supply are difficult. In our previous studies, we experimentally showed that the KC could transport water vapor, which is a condensable gas [26]. Then, a one-dimensional prediction model for gas transport performance was constructed for a multi-stage KC [28]. After evaporation and condensation were incorporated into this model, the performance of a practical heat pump was estimated [27]. In this study, we constructed a KHP demonstration prototype to exhibit its actual operation. In the KHP, a single-stage KC was employed for simplicity and was powered by an indirect heat source, light from a halogen lamp, to show the possibility of solar radiation as an energy source. The performance of the KHP, specifically the output power and temperature difference between the evaporator and condenser, were evaluated from the time variation of the measured pressure and temperature for the evaporator and the condenser. The relationship between the output power and the temperature difference was also investigated.

2 Design of KHP

The KC is a thermally driven compressor without moving parts that utilizes thermal transpiration, a unique phenomenon in a system with a high-Knudsen-number flow. The thermal transpiration is induced by momentum exchange during collisions between gas molecules and a wall. As shown in Fig. 1a, when there is a temperature gradient along a wall, a molecule from the higher-temperature side has a larger momentum than a molecule from the lower-temperature side. Thus, statistically, the wall gains momentum in the direction from higher to lower temperature by gas-surface collisions, resulting in a flow in the gas phase from the lower to higher temperature side. The Knudsen number *Kn* represents the degree of rarefaction of gas, and *Kn* for a gas flow in a channel is expressed as the ratio of the mean free path l for the gas to the characteristic length of the channel D. The basic component of the KC is a material containing micropores (a bundle of microchannels) whose internal *Kn* is 0.1 or more. To create a temperature difference, ΔT_{KC}, across the porous material, one side of the porous material is heated to T_H by light from a halogen lamp through a window, and the other side is cooled to T_L by a heat sink to increase heat dissipation.

The configuration of a KHP using the KC is shown in Fig. 1b. Two chambers, referred to hereafter as the evaporator and condenser, are filled with water as a refrigerant. The evaporator and condenser are connected to each other by two channels to form a refrigerant flow loop. The channel containing the vapor phase comprises the KC, and the other channel containing the liquid phase has a capillary tube. A heat exchanger is installed in each chamber to exchange heat between the inside and outside of the system.

When the KC is in operation [27], vapor is forced to flow from the evaporator to the condenser by the KC. In the evaporator, the pressure drop due to the flow induced by the KC promotes water evaporation, following heat absorption due to the latent heat of water. Then, the temperature in the evaporator, T_E, decreases corresponding to the pressure decrease in the evaporator, P_E, according to the saturated vapor pressure curve for water. In contrast, in the condenser, the pressure increase promotes vapor condensation and heat generation. Then, the temperature in the condenser, T_C, increases corresponding to the pressure increase in the evaporator, P_C. Liquid water returns from the condenser to the evaporator through the capillary tube due to the pressure difference (it can also be assisted by gravity). Since the density of liquid water is much larger than that of water vapor, the pressure change due to water movement can be ignored.

Given this operating mechanism, the performance of the KHP strongly depends on that of the KC. The temperature difference obtained in the KHP, ΔT_{HP}, depends on the pressure difference generated by the KC. The pressure difference can be amplified by cascading KC units [28]. A temperature gradient in the opposite direction to the inside of the porous material occurs at the connection parts of KC unit, but there is no net reverse thermal transpiration occurs if the diameter of the connection part is sufficiently larger than the mean free path. Meanwhile, the output power (heat absorption or generation rate), Q, depends on the mass flow rate of vapor through the KC, which can be increased by enlarging the area of the porous material in the KC.

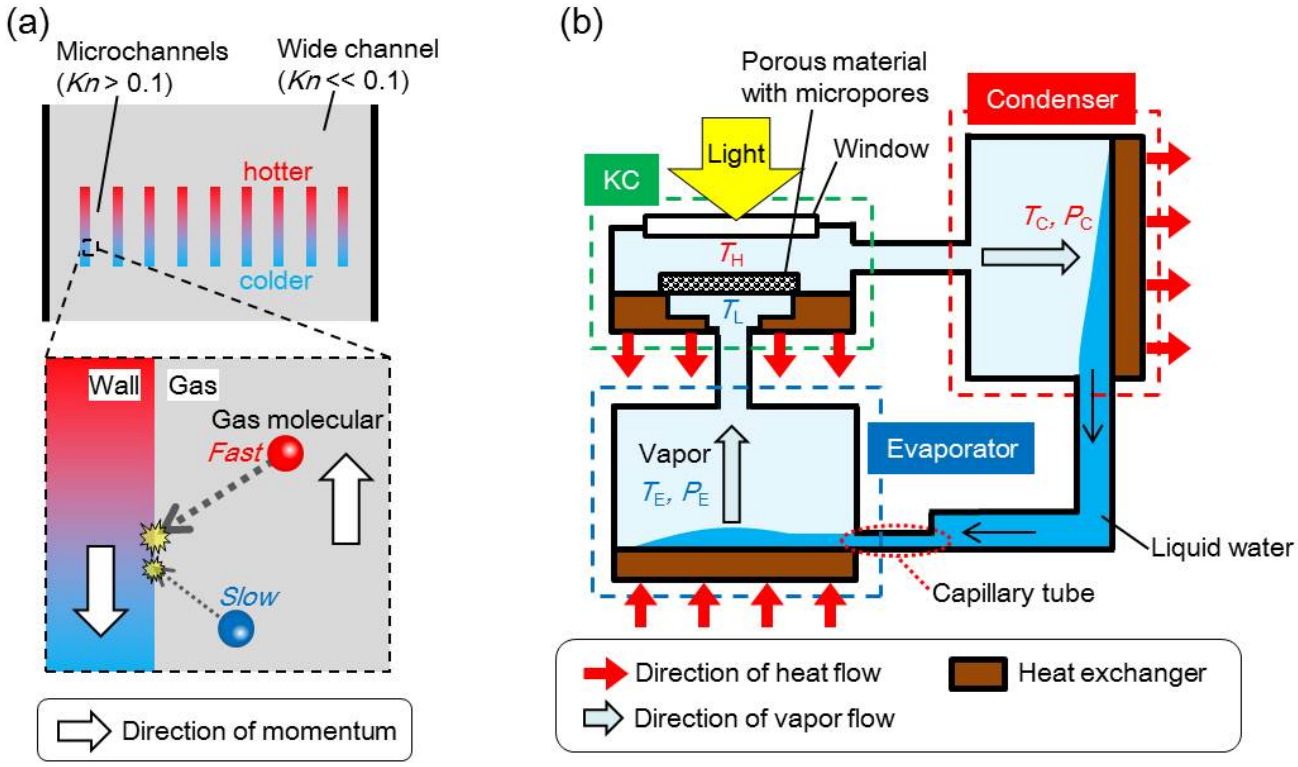

Fig. 1. Design of KHP. (a) Momentum exchange between gas molecules and wall in microchannel. Thermal transpiration is induced by gaining the momentum of gas molecules from the lower to higher temperature side. (b) Schematic of KHP.

3 Methodology

The purpose of this study is to demonstrate the operation of a KHP using the KC powered by light and evaluate its heat pump performance. Therefore, the temperature changes due to heat absorption in the evaporator and heat generation in the condenser are measured, and the liquid water holding state in the evaporator are visualized. In the evaluation of the heat pump performance, the temperatures of the heat transport medium flowing through the heat exchanger in the evaporator and the condenser are changed, and the output powers of the evaporator and the condenser are obtained. From these results, the relationship between the temperature, ΔT_{HP}, and the output power, Q, is investigated. In these experiments, the liquid water is introduced to the evaporator, but not returned from the condenser to the evaporator by installing a valve instead of a capillary tube.

3.1. Demonstration of KHP operation

Figure 2 shows a schematic diagram of the overall KHP experimental apparatus, and Fig. 3a shows the KHP prototype constructed to demonstrate its operation. The KC, evaporator, and condenser are connected in a loop with vacuum pipes, and a valve (26 in Fig. 2) is installed between the evaporator and condenser. A vacuum pump (5) and water tank (4) are connected to the loop for replacing air in the loop with water vapor and supplying liquid water to the evaporator before the measurements. The pressures in the evaporator and the condenser are measured with capacitance manometers (23 and 24). The accuracy of these capacitance manometers (Setra; 730G-010T) is ± 0.15% of full scale, and the full scale of 730G-010T is 1.3 kPa. The manometers are calibrated and checked to be equal before the experiments. A viewport (28) is installed to visually check the holding state of water in the evaporator.

Figure 3b shows the constructed KC. A glass fiber filter (Millipore; APFF) is used as a porous material. The average pore size, thickness, area, and heatproof temperature for the filter are 0.70 μm, 380 μm, 78.5 cm^2, and 773 K, respectively. To increase the temperature difference across the porous material, two filters are stacked. The filters have a circular shape with a diameter of 114 mm, and the outer filter fringe are adhered to the heat exchanger, resulting in thermal transpiration in an area of the central region having a diameter of 100 mm. The surface of one filter is coated with a black pigment to absorb light. A temperature difference across the porous material is created by heating one side with a halogen lamp (3) though the window (2) and cooling the other with a heat exchanger (6). The temperature of the heat transport medium (liquid water) flowing through the heat exchanger (6) is controlled by a temperature control device (12) and is measured with a thermocouple (16) at the outlet of the heat exchanger (6). Also, the temperature of the surface of the porous material is measured with a thermocouple (15). The Class 2 Type K thermocouples used in this study are calibrated at room temperature.

The heat exchangers (7 and 8) of the evaporator and the condenser consist of a copper plate 45 mm square with fine grooves at the center for holding liquid water and a manifold of polyether ether ketone (PEEK). In the evaporator, the water evaporates in the fine grooves, while in the condenser, the water vapor condenses. The latent heat of the phase change of water is transferred to the heat transport medium flowing on the opposite side of the copper plate. The temperatures of the heat transport medium are controlled by temperature control devices (Julabo; F12-MA) (13 and 14) and measured with thermocouples (17-20) at the inlet and the outlet of the heat exchangers (7 and 8), and the flow rates are measured with flow sensors (21 and 22) at the outlet. The accuracy of the flow sensor (Aichi tokei denki; OF05ZAT) is ± 2% of reading scale.

The experimental procedure is as follows. The temperature control devices for the KC, evaporator, and condenser are set to T_K^0, T_E^0, and T_C^0, respectively. The interior of the KC, evaporator, and condenser is evacuated by a vacuum pump. An appropriate amount of liquid water is supplied to fill the interior of the system with water vapor and confine liquid water to the fine grooves of the evaporator only. Then, time series data for the pressures of the evaporator, P_E, and the condenser, P_C, and the temperatures of the heat transport medium at the inlets of the evaporator, T_{EI}, and condenser, T_{CI}, and the outlets of the evaporator, T_{EO}, and condenser, T_{CO}, and KC, T_L, and the temperature of the surface of the porous material, T_H, are recorded before, during, and after irradiation with the halogen lamp. The average values of 60 consecutive data before irradiation are represented by subscript (OFF), and those during irradiation are represented by subscript (ON). The valve is closed during the experiments. All of the measured values are explained in Fig. 4.

In this experiment, T_K^0, T_E^0, and T_C^0 are set to 293.15, 278.15 and 278.35 K, respectively, and the mass flow rates for the evaporator, $\dot{M}_E$, and condenser, $\dot{M}_C$, are set by the volume flow rate of 8.40 and 8.36 cm^3/s, respectively, with the density of water as 1.00 g/cm^3 at 278.15 K [29]. The value for T_E^0 should be lower than the T_C^0 and T_K^0 values to prevent the water supplied to the evaporator from condensing in the condenser or KC.

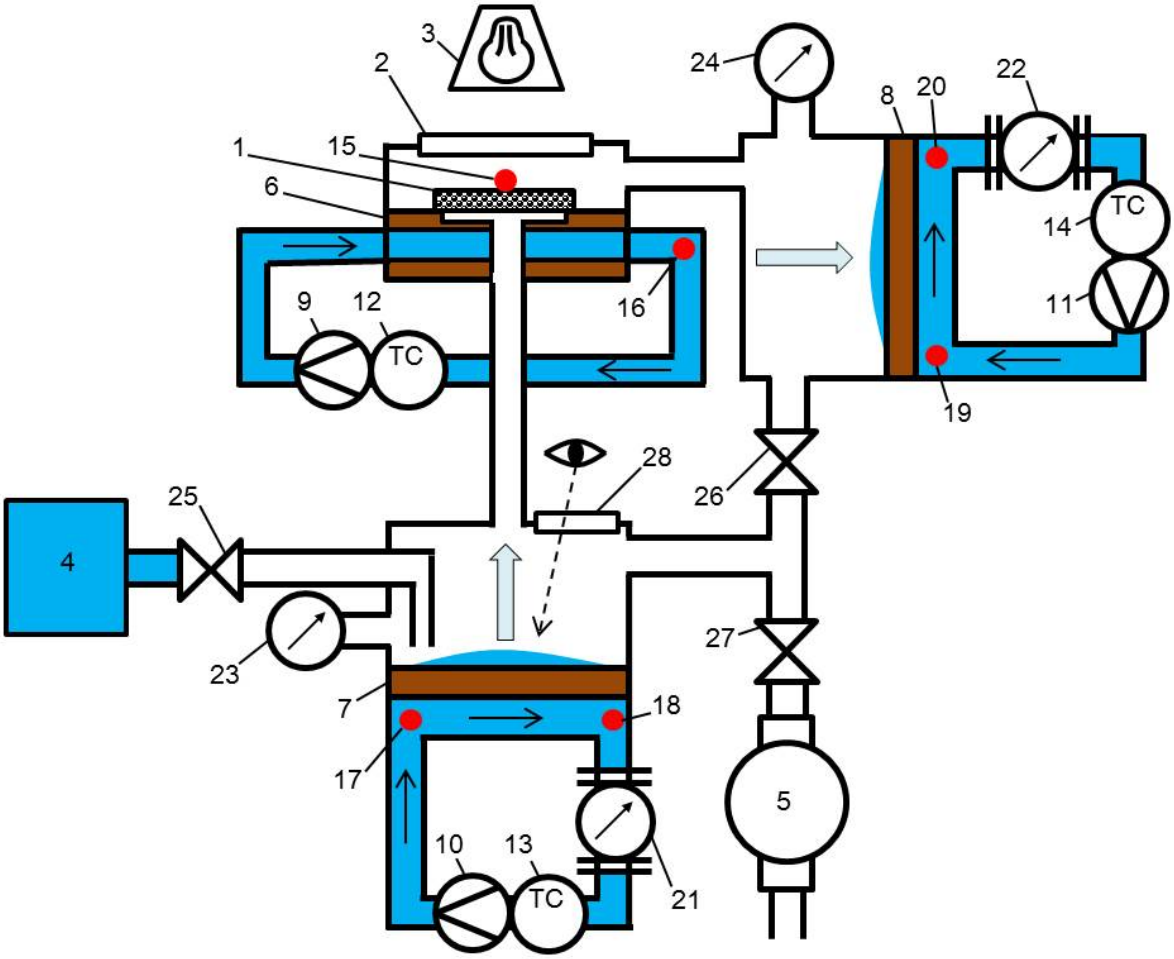

1: glass fiber filters with light absorber
2: glass window
3: halogen lamp
4: water supply tank
5: vacuum pump
6-8: heat exchanger
9-11: liquid pump
12-14: temperature control device
15-20: thermocouple
21, 22: flowmeter
23, 24: manometer
25-27: valve
28: viewport

Fig. 2. Schematic diagram of the whole experimental apparatus of the KHP.

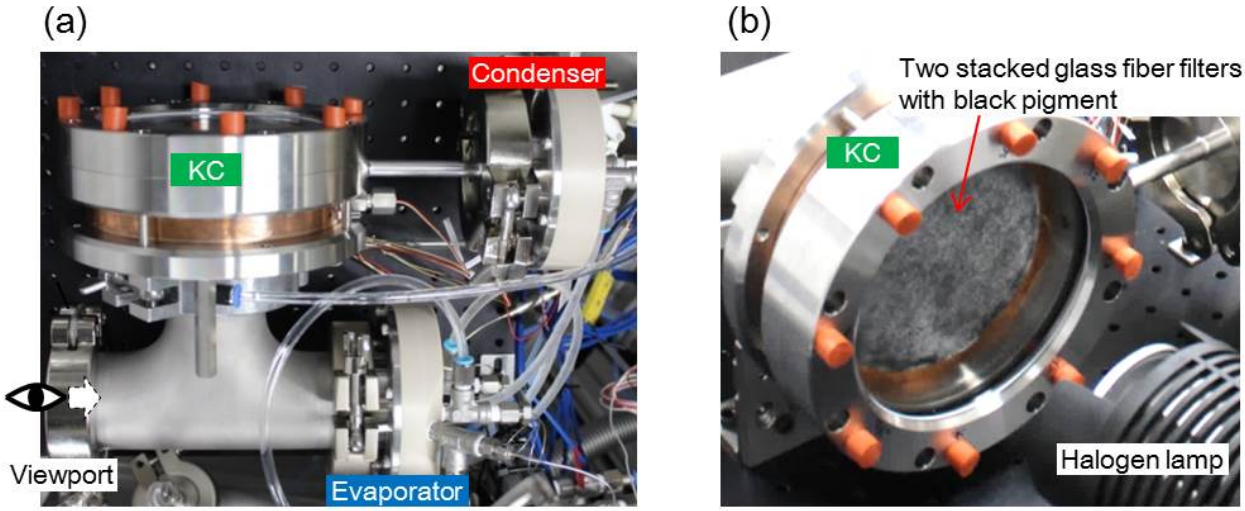

Fig. 3. Experimental KHP with KC used to demonstrate its operating principle. (a) Photograph of the KHP. The heat absorbed and generated in the evaporator and condenser was transferred to the heat transport medium flowing through each heat exchanger and the temperature of the heat transport medium was measured by thermocouples. The pressure in the evaporator and condenser was measured with capacitance manometers. (b) Photograph of KC and halogen lamp heat source. One side of the two stacked glass fiber filters was heated through the window, and the other side was cooled by a heat exchanger.

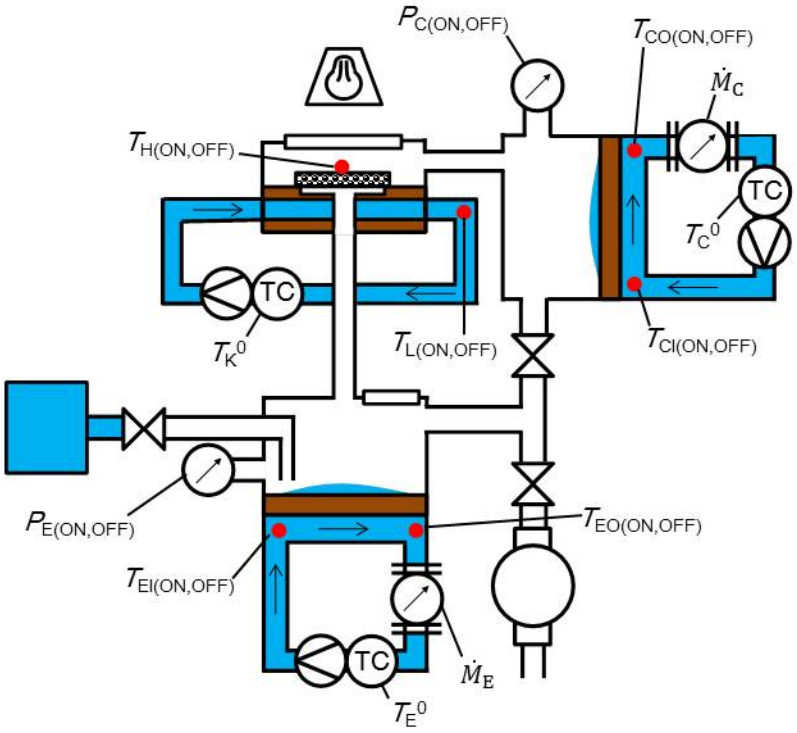

Fig. 4. Parameters measured in this experiment. The average values of 60 consecutive data before irradiation are represented by subscript (OFF), and those during irradiation are represented by subscript (ON).

3.2. Measurement and evaluation of performance of KHP

Next, the relationship between the temperature difference ΔT_{HP} and the output power Q is investigated by changing the temperature settings (T_E^0, T_C^0) to (278.15 K, 278.35 K), (278.05 K, 278.45 K), (277.95 K, 278.55 K), (277.85 K, 278.65 K), and (277.75 K, 278.75 K). The calculation methods of Q and ΔT_{HP} are shown below.

Theoretically, Q is the product of the specific heat c, the mass flow rate $\dot{M}_E$ or $\dot{M}_C$ of the heat transport medium, and the difference between the temperatures at the inlet and the outlet during irradiation, that is, $\Delta T_{EIO(ON)} = T_{EO(ON)} - T_{EI(ON)}$ and $\Delta T_{CIO(ON)} = T_{CO(ON)} - T_{CI(ON)}$. However, Q calculated this way includes the influences of the error in each thermocouple measurement and the inflow of heat from the environment. These influences can be excluded by subtracting the difference between the temperatures at the inlet and the outlet during in the absence of irradiation, $\Delta T_{EIO(OFF)} = T_{EO(OFF)} - T_{EI(OFF)}$ and $\Delta T_{CIO(OFF)} = T_{CO(OFF)} - T_{CI(OFF)}$, from that during irradiation. Thus, the output powers for the evaporator, Q_E, and condenser, Q_C, are calculated by the following equations.

$$Q_E = c\dot{M}_E(\Delta T_{EIO(ON)} - \Delta T_{EIO(OFF)}), \quad (1)$$

$$Q_C = -c\dot{M}_C(\Delta T_{CIO(ON)} - \Delta T_{CIO(OFF)}). \quad (2)$$

Here, c is the specific heat of water of 4.20 J/(g·K) at 278.15 K [29].

The temperature difference between the evaporator and condenser during irradiation, $\Delta T_{HP} = T_{C(ON)} - T_{E(ON)}$, is obtained from the pressure data for $P_{E(ON)}$ and $P_{C(ON)}$ during irradiation. Here, the temperatures of the evaporator, $T_{E(ON)}$, and condenser, $T_{C(ON)}$, correspond to the surface temperature of each copper plate on the side where the fine grooves are present. Thus, $T_{E(ON)}$ and $T_{C(ON)}$ could be different from $T_{EI(ON)}$, $T_{CI(ON)}$, $T_{EO(ON)}$, and $T_{CO(ON)}$. According to Antoine's equation, which gives the saturated vapor pressure of water, $T_{E(ON)}$ and $T_{C(ON)}$ can be related to the pressure $P_{E(ON)}$ and $P_{C(ON)}$ as follows:

$$\log_{10}(\kappa P_i) = \alpha - \frac{\beta}{T_i - \gamma}, \ (i = \text{E(ON) and C(ON)}), \quad (3)$$

where, κ, α, β, and γ are constants that depend on substances and units. In the case of water vapor, when using pascals as the units for pressure P_i and kelvins as the units for temperature T_i, $\kappa = 10^{-3}$ Pa^{-1}, $\alpha = 7.17\times10^{0}$, $\beta = 1.72\times10^{3}$ K, and $\gamma = 4.06\times10^{1}$ K [30].

4 Results

4.1 Demonstration of KHP operation

Figure 5a shows time series data for T_H and T_L. The halogen lamp was turned on 120 s after the start of data recording, and it was turned off after 240 s. Since the heat capacity of the porous material was small, T_H changed quickly due to the presence and absence of irradiation, and reached an almost steady state in 10 s. In contrast, T_L was almost constant despite irradiation. During irradiation, $T_{H(ON)}$ and $T_{L(ON)}$ were 494.77 and 294.46 K, respectively, and the temperature difference across the porous materials $\Delta T_{KC(ON)} = T_{H(ON)} - T_{L(ON)}$ was 200.31 K.

Figure 5b shows time series data for P_E and P_C, and Fig. 5c shows the results for T_{EI}, T_{CI}, T_{EO}, and T_{CO}. After turning on the halogen lamp, P_E and T_{EO} decreased in the evaporator, while P_C and T_{CO} increased in the condenser. All of these returned to their initial values after the lamp was turned off. During the measurement, T_{EI} and T_{CI} were almost constant. Thus, it is reasonable to consider that the changes in P_E and P_C were due to water vapor transport by the KC, and the changes in T_{EO} and T_{CO} were due to latent heat of evaporation and condensation, respectively. After irradiation, Pc did not immediately return to its initial value. This is considered to be because liquid water still remained in the condenser after irradiation, and it evaporated very slowly.

Here, an irradiation experiment was separately conducted for over 10 min in order to visually check the time evolution of the evaporation of water in the evaporator. Figure 6 shows the holding state of liquid water in the evaporator. Before light irradiation, the fine grooves were wet, but 10 min after irradiation, the water had evaporated and the surface was dry. These results confirmed the successful operation of the KHP.

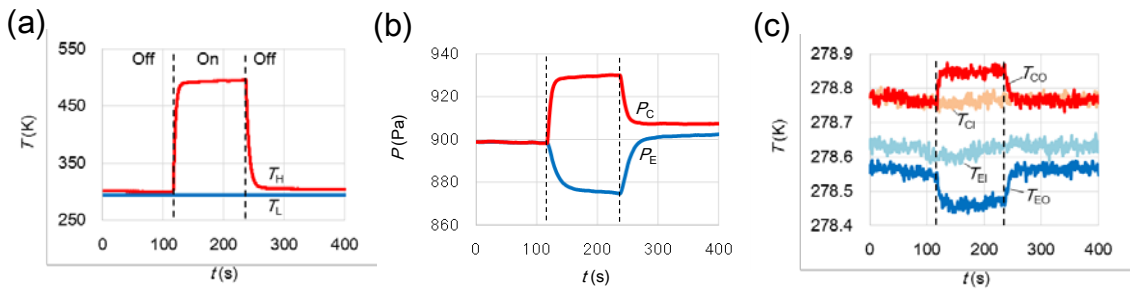

Fig. 5. Results at (T_E^0, T_C^0) = (278.15 K, 278.35 K). (a) Time series data for T_H and T_L. The halogen lamp was turned on 120 s after the start of data recording and turned off after 240 s. (b) Time series data for P_E and P_C. (c) Time series data for T_{EI}, T_{CI}, T_{EO}, and T_{CO}.

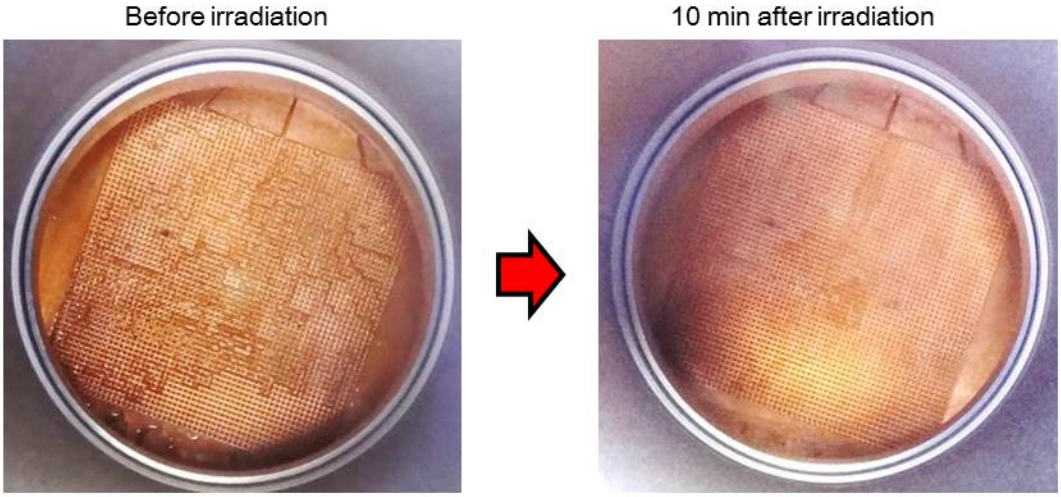

Fig. 6. State of liquid held in the evaporator before and after light irradiation for 10 min. Before light irradiation, the fine grooves were wet; after 10 min of irradiation, water had evaporated and the surface was dry.

4.2 Relationship between temperature difference ΔT_{HP} and output power Q

Time series data for T_H, T_L, P_E, P_C, T_{EI}, T_{CI}, T_{EO}, and T_{CO} for the temperature settings (T_E^0, T_C^0) to (278.05 K, 278.45 K), (277.95 K, 278.55 K), (277.85 K, 278.65 K), and (277.75 K, 278.75 K) are shown in Fig. 7. From the data in Fig.7, $T_{H(ON)}$, $T_{L(ON)}$, $\Delta T_{KC(ON)}$, $P_{E(ON)}$, $P_{C(ON)}$, $\Delta T_{EIO(ON)}$ - $\Delta T_{EIO(OFF)}$, and $\Delta T_{CIO(ON)}$ - $\Delta T_{CIO(OFF)}$ for each (T_E^0, T_C^0) are obtained, and these are listed in Table 1. The values of $P_{C(ON)}$ - $P_{E(ON)}$, $\Delta T_{EIO(ON)}$ - $\Delta T_{EIO(OFF)}$, and $\Delta T_{CIO(ON)}$ - $\Delta T_{CIO(OFF)}$ decreased as T_C^0 - T_E^0 increased. T_H (T_L) shows similar profiles with respect to (T_E^0, T_C^0). The time for P_E and P_C to return to the initial value after

irradiation was shorter as T_C^0 - T_E^0 was larger. This is considered to be because the amount of condensed water decreased with increase in T_C^0 - T_E^0.

The heat pump performances of $T_{E(ON)}$, $T_{C(ON)}$, ΔT_{HP}, Q_E, and Q_C for each (T_E^0, T_C^0) are listed in Table 2. Figure 8 shows the relationship between ΔT_{HP}, Q_E, and Q_C. As shown in Table 2 and Fig. 8, the values of Q_E and Q_C are almost the same. Again from the figure, Q_E and Q_C tend to increase linearly as ΔT_{HP} decreases, which was predicted by the performance simulation of the KHP in our previous study [27]. Therefore, the concept of the KHP has been demonstrated not only qualitatively but also quantitatively. An approximate function for this relation can be expressed as follows:

$$Q = Q_{MAX}\left(1 - \frac{\Delta T_{HP}}{\Delta T_{HPMAX}}\right), \tag{4}$$

where Q_{MAX} and ΔT_{HPMAX} are the maximum output power and maximum temperature difference, respectively, which in the present study were determined to be 8.23 W and 1.37 K, respectively.

The maximum temperature difference ΔT_{HPMAX} can be increased by using a multi-stage KC [27]. The previous study indicated that Q_{MAX} and ΔT_{HPMAX} in Eq. (4) increase roughly in proportion to the area of the porous material and the number of stages in a multi-stage KC, respectively. From the results of this study, it is estimated that Q_{MAX} and ΔT_{HPMAX} become 2.0 kW and 21 K by using a 15-stage KC with each stage having a porous area of 1.9 m^2, thus a performance of Q = 1.0 kW at ΔT_{HP} = 10 K can be obtained.

The standard errors of the average values of 60 consecutive data were obtained for the measured conditions to evaluate uncertainties. Table 3 shows the standard errors for $T_{H(ON)}$, $T_{L(ON)}$, $P_{E(ON)}$, $P_{C(ON)}$, $\Delta T_{EIO(ON)}$ - $\Delta T_{EIO(OFF)}$, and $\Delta T_{CIO(ON)}$ - $\Delta T_{CIO(OFF)}$ for each (T_E^0, T_C^0). The standard errors for $T_{H(ON)}$, $T_{L(ON)}$, $P_{E(ON)}$, and $P_{C(ON)}$ are sufficiently smaller than the accuracy of the pressure gauges and thermocouples used in this experiment. The uncertainties of these values are evaluated from the accuracies of measurement devices and the standard errors. As for $\Delta T_{EIO(ON)}$ - $\Delta T_{EIO(OFF)}$ and $\Delta T_{CIO(ON)}$ - $\Delta T_{CIO(OFF)}$ in Q, since these values are very small, the temperature fluctuation of the temperature control devices, which can be usually neglected, would lead to the measurement error, so the standard deviation of the fluctuation is also included. The total uncertainties of ΔT_{KC}, ΔT_{HP}, and Q are evaluated and listed in Table 1 and 2. The uncertainties for each condition are shown by the error bars in Fig. 8.

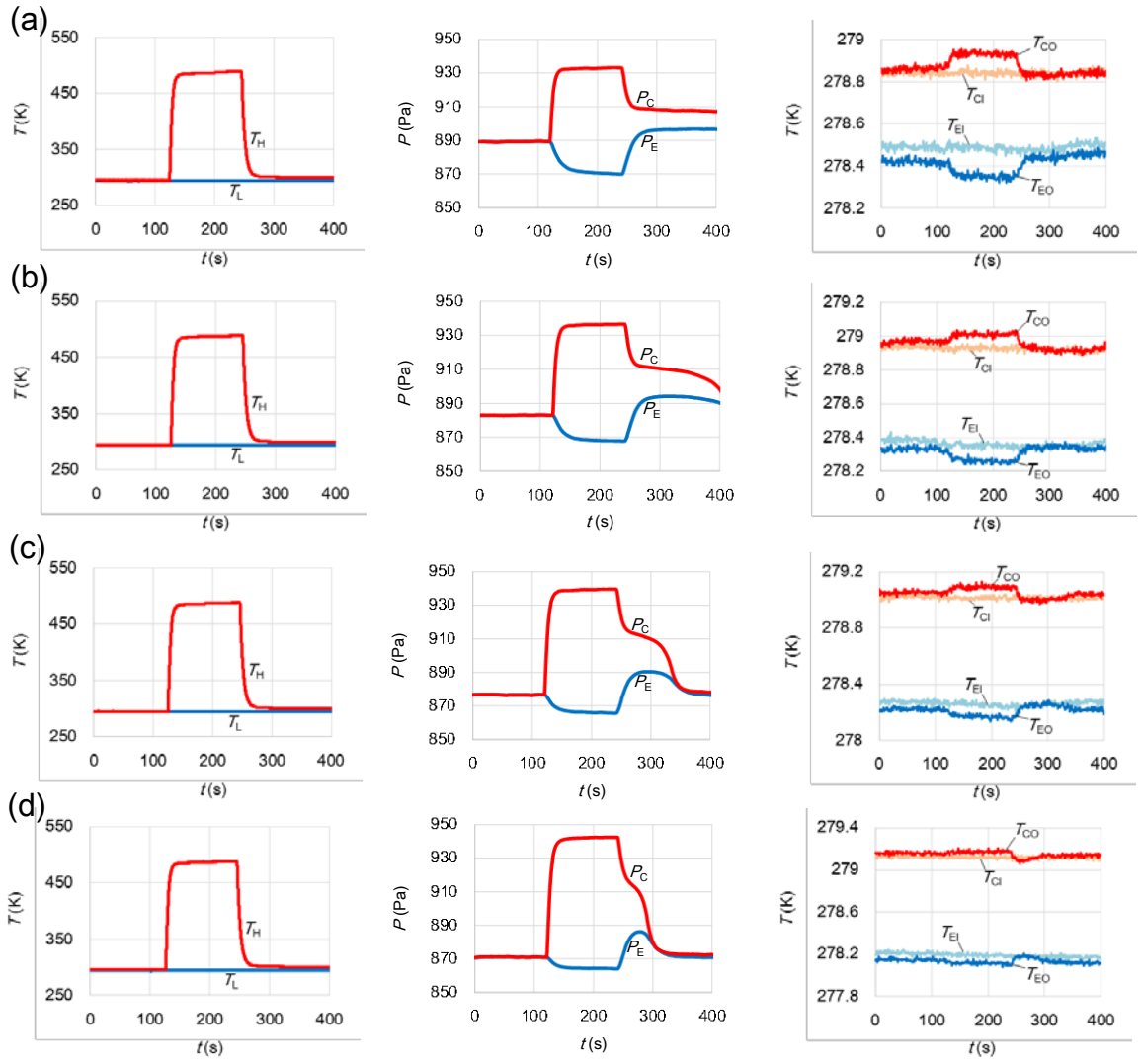

Fig. 7. Time series data for T_H, T_L, P_E, P_C, T_{EI}, T_{CI}, T_{EO}, and T_{CO}. (a) At (T_E^0, T_C^0) = (278.05 K, 278.45 K). (b) At (T_E^0, T_C^0) = (277.95 K, 278.55 K). (c) At (T_E^0, T_C^0) = (277.85 K, 278.65 K). (d) At (T_E^0, T_C^0) = (277.75 K, 278.75 K).

Table 1

$T_{H(ON)}$, $T_{L(ON)}$, $\Delta T_{KC(ON)}$, $P_{E(ON)}$, $P_{C(ON)}$, $\Delta T_{EIO(ON)}$ - $\Delta T_{EIO(OFF)}$, and $\Delta T_{CIO(ON)}$ - $\Delta T_{CIO(OFF)}$ for different (T_E^0, T_C^0) combinations.

T_E^0 (K), T_C^0 (K)	$T_{H(ON)}$ (K)	$T_{L(ON)}$ (K)	$\Delta T_{KC(ON)}$ (K)	$P_{E(ON)}$ (Pa)	$P_{C(ON)}$ (Pa)	$\Delta T_{EIO(ON)}$ - $\Delta T_{EIO(OFF)}$ (K)	$\Delta T_{CIO(ON)}$ - $\Delta T_{CIO(OFF)}$ (K)
278.15, 278.35	494.77	294.46	200.31 ±1.50	876	930	0.0874	0.0819
278.05, 278.45	488.71	294.56	194.16 ±1.45	871	933	0.0671	0.0668
277.95, 278.55	488.52	294.60	193.92 ±1.46	868	936	0.0505	0.0450
277.85, 278.65	488.03	294.54	193.49 ±1.45	866	939	0.0303	0.0437
277.75, 278.75	487.93	294.43	193.50 ±1.45	864	942	0.0151	0.0222

Table 2

Heat pump performance for $T_{E(ON)}$, $T_{C(ON)}$, ΔT_{HP}, Q_E, and Q_C for different (T_E^0, T_C^0) combinations.

T_E^0 (K), T_C^0 (K)	$T_{E(ON)}$ (K)	$T_{C(ON)}$ (K)	ΔT_{HP} (K)	Q_E (W)	Q_C (W)
278.15, 278.35	278.26	279.12	0.859 ±0.004	3.09 ±0.31	2.88 ±0.26
278.05, 278.45	278.18	279.17	0.990 ±0.004	2.37 ±0.18	2.35 ±0.22
277.95, 278.55	278.14	279.22	1.084 ±0.004	1.78 ±0.31	1.58 ±0.22
277.85, 278.65	278.10	279.27	1.166 ±0.005	1.07 ±0.18	1.53 ±0.18
277.75, 278.75	278.07	279.31	1.240 ±0.005	0.53 ±0.23	0.78 ±0.18

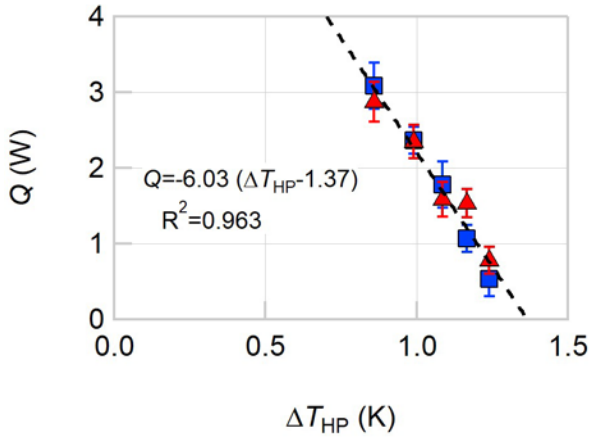

Fig. 8. Relationship between ΔT_{HP} and Q. Blue squares and red triangles represent Q_E and Q_C, respectively. The black dashed line indicates a linear approximation function. The uncertainties for each condition are shown by the error bars.

Table 3
The standard errors of the average values of 60 consecutive data for $T_{H(ON)}$, $T_{L(ON)}$, $P_{E(ON)}$, $P_{C(ON)}$, $\Delta T_{EIO(ON)}$ - $\Delta T_{EIO(OFF)}$, and $\Delta T_{CIO(ON)}$ - $\Delta T_{CIO(OFF)}$ for different (T_E^0, T_C^0) combinations.

T_E^0 (K), T_C^0 (K)	for $T_{H(ON)}$ (K)	for $T_{L(ON)}$ (K)	for $P_{E(ON)}$ (Pa)	for $P_{C(ON)}$ (Pa)	for $\Delta T_{EIO(ON)}$ - $\Delta T_{EIO(OFF)}$ (K)	for $\Delta T_{CIO(ON)}$ - $\Delta T_{CIO(OFF)}$ (K)
278.15, 278.35	0.0152	0.00418	0.0500	0.0544	0.00326	0.00261
278.05, 278.45	0.00920	0.00576	0.0387	0.0618	0.00310	0.00281
277.95, 278.55	0.0173	0.00964	0.0267	0.0525	0.00302	0.00260
277.85, 278.65	0.00817	0.0102	0.0385	0.0503	0.00270	0.00265
277.75, 278.75	0.0156	0.00801	0.0338	0.0428	0.00286	0.00243

4.3 Theoretical analysis of thermal efficiency of KHP

4.3.1. KHP with single-stage KC

The thermal efficiency of the KHP is analyzed. Figure 9 shows the pressure-enthalpy diagram of a KHP cycle with a single-stage KC when the change of the refrigerant from the condenser to the evaporator is adiabatic expansion. The red bold solid line, black solid lines, and black dash lines represent the KHP cycle, saturated liquid and steam lines, and isothermal lines of T_H and T_L, respectively [31]. The saturated vapor of T_E and P_E at evaporator (state 1 in Fig. 9) is heated by the heat exchanger to become the super-heated vapor of T_L and P_E at the inlet of the KC (state 2). The super-heated vapor is heated and pressurized by the KC to become the super-heated vapor of T_H and P_C at the outlet of the KC (state 3). The super-heated vapor is cooled by heat dissipation to the saturated vapor of T_C and P_C at condenser (state 4). The saturated vapor is condensed to the saturated liquid water of T_C and P_C in condenser (state 5). The saturated liquid water is depressurized by adiabatic expansion to the liquid-vapor mixture of T_E and P_E in evaporator (state 6). The liquid-vapor mixture is, then, evaporated to become the saturated vapor of the state 1.

On standard refrigerating cycle, the heat absorption in the evaporator Q, the work for compression U_{work}, and the coefficient of performance η_i are defined as follows with the mass flow rate of water vapor $\dot{M}_V$ and the specific enthalpies h_2, h_3, h_6 of the states 2, 3, 6.

$$Q = \dot{M}_V (h_2 - h_6), \tag{5}$$

$$U_{work} = \dot{M}_V (h_3 - h_2), \tag{6}$$

$$\eta_i = \frac{Q}{U_{work}} = \frac{h_2 - h_6}{h_3 - h_2}. \tag{7}$$

The value of η_i of this experiment is estimated. When T_H = 494.77 K, T_L = 294.46 K, T_E = 278.26 K, T_C = 279.12 K, P_E = 875 Pa, P_C = 930 Pa, and Q = 3.09 W shown in the first condition of Table 1 and 2, $\dot{M}_V$, h_2, h_3, and h_6 are calculated as 1.23 mg/s, 2541 kJ/kg, 2922 kJ/kg, and 25 kJ/kg, respectively, then U_{work} can be obtained as 0.47 W. Thus, η_i is 6.61.

In practice, the temperature difference across the porous material in the KC must be maintained. Therefore, it is necessary to continue to input not only energy used for work but also energy lost by radiation to the surrounding environment from the high temperature side and the heat conduction through the porous material. The energy lost by radiation $U_{radiation}$ and the energy lost by heat conduction $U_{conduction}$ can be expressed by the following equations.

$$U_{\text{radiation}} = \sigma \varepsilon A\left(T_H^4 - T_{RT}^4\right), \tag{8}$$

$$U_{\text{conduction}} = \frac{\lambda A\left(T_H - T_L\right)}{d}. \tag{9}$$

Here, σ, ε, λ, A, d, and T_{RT} are the Stefan–Boltzmann constant, emissivity, thermal conductivity, area and thickness of porous material, and room temperature, respectively. The thermal conductivity of the porous material generally depends on the pressure and the temperature [32]. The energy practically required for driving KHP U_{all} is as follows.

$$U_{\text{all}} = U_{\text{work}} + U_{\text{radiation}} + U_{\text{conduction}}. \tag{10}$$

Therefore, the practical coefficient of efficiency η_p is as follows.

$$\eta_p = \frac{Q}{U_{\text{all}}}. \tag{11}$$

To estimate the value of η_p of this experiment, the thermal conductivity of a general glass fiber filter at 1 kPa and 324 K is known to be about 0.03 W/(m·K) [32]; thus λ = 0.03 W/(m·K) is employed. When ε = 1, A = 78.5 cm^2, d = 0.76 mm, T_{RT} = T_L = 294.37 K shown in the first condition of Table 1 and 2**,** $U_{radiation}$ and $U_{conduction}$ are calculated to be 23.3 W and 62.1 W; then U_{all} is obtained as 85.9W, resulting in η_p = 0.036. $U_{radiation}$ and $U_{conduction}$ are much larger than U_{work} in this estimation. The issue for the future is to reduce $U_{radiation}$ and $U_{conduction}$ through optimization of a light absorber and porous material.

Figure 11 shows the coefficient of performance η_i, η_p shown in the Table 1 and 2 on standard refrigerating cycle. As shown in Fig. 8, as ΔT_{HP} increases, the output power Q, i.e. the mass flow rate of water vapor $\dot{M}_V$, decreases. Since η_i does not depend on the mass flow rate as in Eq. (7), it hardly changes even if ΔT_{HP} changes. On the other hand, η_p decreases as ΔT_{HP} increases and Q decreases. This is because the heat conduction and radiation loss, which are independent of $\dot{M}_V$, are

quite larger than the work for compression in the present apparatus. In the future, if the heat conduction and radiation loss can be reduced, η_p is considered to approach η_i.

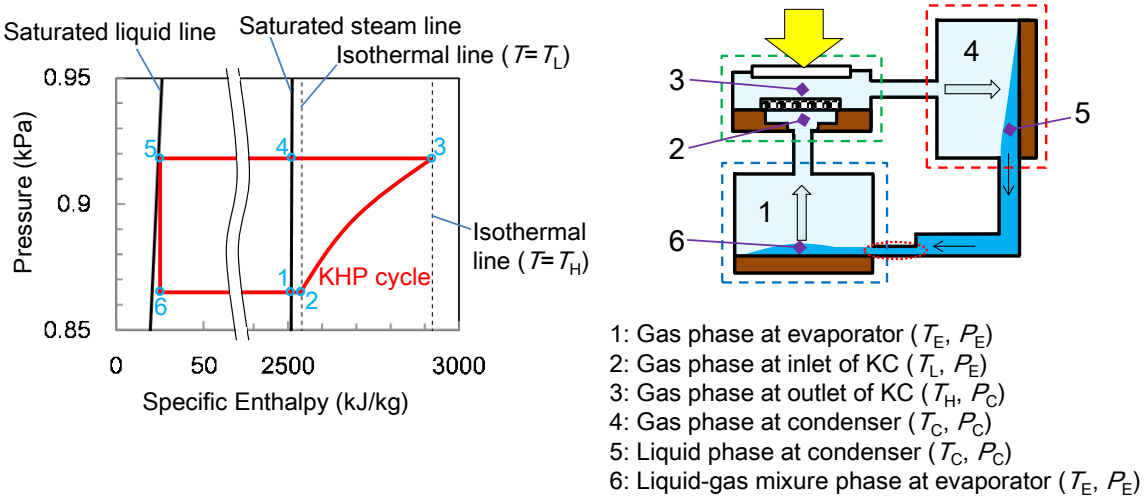

Fig. 9. Pressure-enthalpy diagram of a KHP cycle with a single-stage KC when the change of the refrigerant from the condenser to the evaporator is adiabatic expansion. The cycle, saturated liquid and stream lines, and isothermal lines are plotted by the red bold solid line, black solid lines, and black dash lines, respectively. In this diagram, T_H = 494.77 K, T_L = 294.46 K, T_E = 278.26 K, T_C = 279.12 K, P_E = 875 Pa, P_C = 930 Pa, and Q = 3.09 W shown in the first condition of Table 1 and 2.

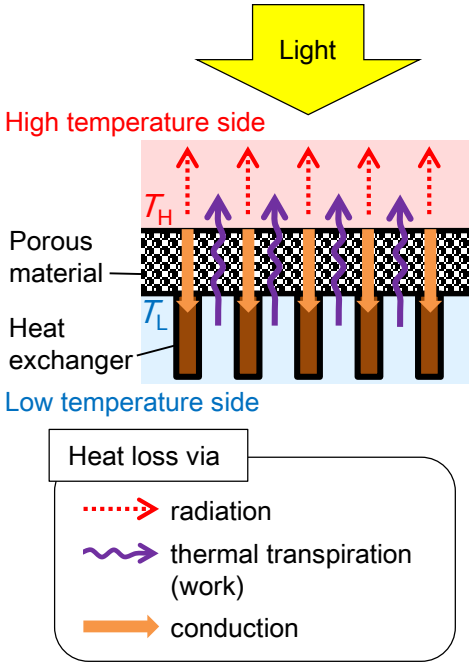

Fig. 10. Schematic of energy required to maintain of the temperature difference across the porous material in KC.

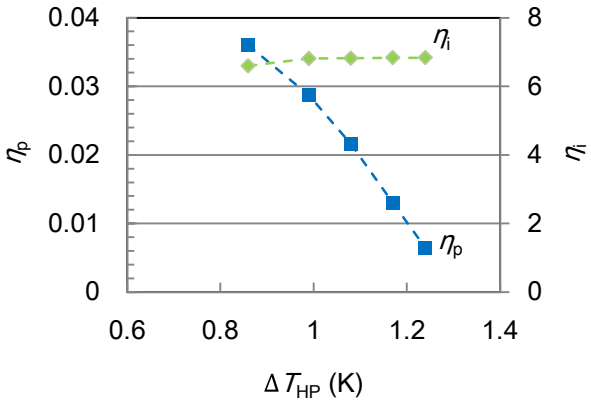

Fig. 11. The coefficient of performance shown in the Table 1 and 2 on standard refrigerating cycle. Blue squares represent η_p on the left axis and green diamonds represent η_i on the right axis.

4.3.2. KHP with multi-stage KC

Next, the thermal efficiency of the KHP with a multi-stage KC is considered. For the pressure-enthalpy diagram of a KHP cycle with a multi-stage KC, the process from state 2 to state 3 will change. Figure 12 shows the pressure-enthalpy

diagram of an example of a KHP cycle with a two-stage KC when the change of the refrigerant from the condenser to the evaporator is adiabatic expansion. The states 2-*n* and 3-*n* on the KHP cycle represent the states of the *n*th-stage KC; thus, the states 2-1, 3-1, 2-2, and 3-2 correspond to the gas phase at the inlet and outlet of 1st KC, and inlet and outlet of 2nd KC, respectively. The super-heated vapor of T_L and P_E at the inlet of the 1st KC (state 2-1) is heated and pressurized by the 1st KC to become the super-heated vapor of T_H and P_M at the outlet of the 1st KC (state 3-1). The super-heated vapor is cooled by heat dissipation to the super-heated vapor of T_L and P_M at the inlet of the 2nd KC (state 2-2). The super-heated vapor is heated and pressurized by the 2nd KC to the super-heated vapor of T_H and P_C at the outlet of the 2st KC (state 3-2). Q and U_{work} for the two-stage KC become as follows with $\dot{M}_V$ and $h_{2\text{-}1}$, $h_{3\text{-}1}$, $h_{2\text{-}2}$, $h_{3\text{-}2}$, h_6 of the states 2-1, 3-1, 2-2, 3-2, 6.

$$Q = \dot{M}_V \left(h_{2\text{-}1} - h_6 \right), \tag{12}$$

$$U_{work} = \dot{M}_V \left(h_{3\text{-}1} - h_{2\text{-}1} + h_{3\text{-}2} - h_{2\text{-}2} \right). \tag{13}$$

Since the values of Q and h_3 - h_2 of each stage weakly change depending on the number of stages, the efficiency of KHP using N-stage KC is approximately $1/N$ of the efficiency of that using a single-stage KC. Therefore, when 15-stage KC is used to obtain a temperature difference of 10 K, η_i of the KHP can be estimated to be approximately 1/15. The heat is merely lost at the connection parts of KCs, which corresponds to the process from state 3-1 to state 2-2 in Fig. 12. Therefore, the heat pump efficiency will rise by recovering this waste heat. Since $U_{radiation}$ and $U_{conduction}$ also increase in proportion to the number of stages, it is estimated that η_p of KHP using an N-stage KC is approximately $1/N$ of η_p of KHP using a single-stage KC.

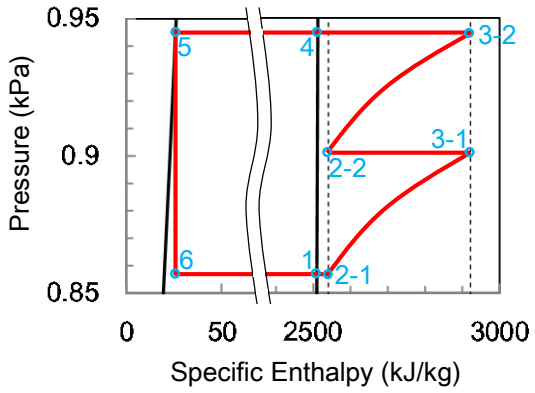

1: Gas phase at evaporator (T_E, P_E)
2-1: Gas phase at inlet of 1st KC (T_L, P_E)
3-1: Gas phase at outlet of 1st KC (T_H, P_M)
2-2: Gas phase at inlet of 2nd KC (T_L, P_M)
3-2: Gas phase at outlet of 2nd KC (T_H, P_C)
4: Gas phase at condenser (T_C, P_C)
5: Liquid phase at condenser (T_C, P_C)
6: Liquid-gas mixture phase at evaporator (T_E, P_E)

Fig. 12. Pressure-enthalpy diagram of an example of a KHP cycle with a multi-stage KC (2 stages) when the change of the refrigerant from the condenser to the evaporator is adiabatic expansion. The cycle, saturated liquid and stream lines, and isothermal lines are plotted by the red bold solid line, black solid lines, and black dash lines, respectively.

5 Conclusion

We confirmed that the KC drove pressure and temperature changes in the evaporator and condenser of the KHP. The amount of liquid water in the evaporator was observed to decrease over time. These results confirmed the successful operation of this novel heat pump. To evaluate its performance, the relationship between the temperature difference between the evaporator and the condenser and the output power was clarified by changing the temperature of the evaporator and the condenser. The output power tended to increase linearly as the temperature difference decreased, which was predicted in our previous theoretical study [27]. The performances of the KHP Q at ΔT_{HP} can increase by increasing the area of the porous material and the number of stages in a multi-stage KC. The pressure-enthalpy diagram was shown for the proposed KHP, and the thermal efficiencies of the KHP were analyzed for these experiments. The ideal thermal efficiency estimated from the pressure-enthalpy diagram in this study was about 6.6. However, the practical thermal efficiency was considerably smaller since the heat conduction loss through the porous material and the radiation loss were quite large in this prototype. Further research on a KC unit will be needed for better performance and efficiency. Nevertheless, it is considered that KHP with no moving parts and no vibration has great engineering potential.

Acknowledgments

The authors wish to thank M. Yokoi (TCRDL) for designing the experimental apparatus. We also wish to thank H. Yoshida (TCRDL) for his many suggestions which improved the final paper.

References

1. Staffell, I., Brett, D., Brandon, N., & Hawkes, A. A review of domestic heat pumps. *Energy Environ. Sci.* **5**, 9291–9306 (2012).
2. Wongsuwan, W., Kumar, S., Neveu, P., & Meunier, F. A review of chemical heat pump technology and applications. *Appl. Therm. Eng.* **21**, 1489–1519 (2001).
3. Demira, H., Mobedib, M., & Ülkü, S. A review on adsorption heat pump: Problems and solutions. *Renew. Sust. Energ. Rev.* **12**, 2381–2403 (2008).
4. Aristov, Yu. I., Dawoud, B., Glaznev, I. S., & Elyas, A. A new methodology of studying the dynamics of water sorption/desorption under real operating conditions of adsorption heat pumps: Experiment. *Int. J. Heat Mass Transfer* **51**, 4966–4972 (2008).
5. Restuccia, G., Freni, A., & Maggio, G. A zeolite-coated bed for air conditioning adsorption systems: parametric study of heat and mass transfer by dynamic simulation. *Appl. Thermal Eng.* **22**, 619–630 (2002).
6. Miltkau, T., & Dawoud, B. Dynamic modeling of the combined heat and mass transfer during the adsorption/desorption of water vapor into/from a zeolite layer of an adsorption heat pump. *Int. J. Thermal Sci.* **41**, 753–762 (2002).
7. Critoph, R. E., Metcalf, S. J., & Telto, T. Z. Proof of concept car adsorption air-conditioning system using a compact sorption reactor. *Heat Transfer Eng.* **31**, 950–956 (2010).
8. Sone, Y. *Molecular Gas Dynamics: Theory, Techniques, and Applications* (Birkhäuser, Boston, 2007).
9. Knudsen, M. Eine Revision der Gleichgewichtsbedingung der Gase. Thermische Molekularströmung. *Ann. Phys.* **31**, 205 (1909). [In German]
10. Knudsen, M. Thermischer Molekulardruck der Gase in Röhren. *Ann. Phys.* **33**, 1435 (1910). [In German]
11. Cercignani, C., & Daneri, A. Flow of a rarefied gas between two parallel plates. *J. Appl. Phys.* **34**, 3509 (1963).
12. Ohwada, T., Sone, Y., & Aoki, K. Numerical analysis of the Poiseuille and thermal transpiration flows between two parallel plates on the basis of the Boltzmann equation for hard-sphere molecules. *Phys. Fluids A* **1**, 2042 (1989).
13. Sharipov, F., & Bertoldo, G. Poiseuille flow and thermal creep based on the Boltzmann equation with the Lennard-Jones potential over a wide range of the Knudsen number. *Phys. Fluids* **21**, 067101 (2009).
14. Chen, C. C., Chen, I. K., Liu, T. P., & Sone, Y. Thermal transpiration for the linearized Boltzmann equation. *Commun. Pure Appl. Math.* **60**, 147 (2007).
15. Loyalka, S. K. Thermal transpiration in a cylindrical tube. *Phys. Fluids* **12**, 2301–2305 (1969).
16. Vargo, S. E., Muntz, E. P., Shiflett, G. R., & Tang, W. C. Knudsen compressor as a micro- and macroscale vacuum pump without moving parts or fluids. *J. Vac. Sci. Technol. A* **17**, 2308-2313 (1999).
17. Young, M., Han, Y. L., Muntz, E. P., & Shiflett, G. Characterization and Optimization of a Radiantly Driven Multi-Stage Knudsen Compressor. *AIP Conf. Proc.* **762**, 174 (2005).
18. Liu, J., Gupta, N. K., Wise, K. D., Gianchandani, Y. B., & Fan, X. Demonstration of motionless Knudsen pump based micro-gas chromatography featuring micro-fabricated columns and on-column detectors. *Lab Chip* **11**, 3487 (2011).
19. Qin, Y., & Gianchandani, Y. B. A fully electronic microfabricated gas chromatograph with complementary capacitive detectors for indoor pollutants. *Microsyst. Nanoeng.* **2**, 15049 (2016).
20. Nakaye, S., & Sugimoto, H. Demonstration of a gas separator composed of Knudsen pumps. *Vacuum* **125**, 154-164 (2016).
21. Pharas, K., & McNamara, S. Knudsen pump driven by a thermoelectric material. *J. Micromech. Microeng.* **20**, 125032 (2010).
22. Gerdroodbary, M. B., Anazadehsayed, A., Hassanvand, A., & Moradi, R. Calibration of low-pressure MEMS gas sensor for detection of hydrogen gas. *Int. J. Hydrogen Energy* **43**, 5770-5782 (2018).
23. Gerdroodbary, M. B., Mosavat, M., Ganji, D. D., Taeibi-Rahni, M., & Moradi, R. Application of molecular force for mass analysis of Krypton/Xenon mixture in low-pressure MEMS gas sensor. *Vacuum* **150**, 207-215 (2018).

24. Gerdroodbary, M. B., Ganji, D. D., Taeibi-Rahni, M., & Vakilipour S. Effect of geometrical parameters on radiometric force in low–pressure MEMS gas actuator. *Microsyst. Technol.* **24**, 2189–2198 (2018).
25. An, S., Qin, Y., & Gianchandani, Y. B. A monolithic high-flow Knudsen pump using vertical Al_2O_3 channels in SOI. *J. Microelectromech. Syst.* **24**, 1606 (2015).
26. Kugimoto, K., Hirota, Y., & Kizaki, Y. Motionless heat pump – A new application of thermal transpiration. *AIP Conf. Proc.* **1786**, 080004 (2016).
27. Kugimoto, K., Hirota, Y., Yamauchi, T., Yamaguchi, H., & Niimi, T. A novel heat pump system using a multi-stage Knudsen compressor. *Int. J. Heat Mass Transfer* **127**, 84–91 (2018).
28. Kugimoto, K., Hirota, Y., Yamauchi, T., Yamaguchi, H., & Niimi, T. Performance prediction method for a multi-stage Knudsen pump. *Phys. Fluids* **29**, 122002 (2017).
29. Rumble, J. *CRC Handbook of Chemistry and Physics, 98th Edition* (CRC Press, Boca Raton, 2017).
30. Rodgers, R. C., & Hill, G. E. Equations for vapour pressure versus temperature: Derivation and use of the Antoine equation on a hand-held programmable calculator. *Br. J. Anaesth.* **50**, 415 (1978).
31. JSME *1999 JSME STEAM TABLES* (Maruzen, Tokyo, 1999).
32. Stark, C., & Fricke, J. Improved heat-transfer models for fibrous insulations. *Int. J. Heat Mass Transfer* **36**, 617–625 (1992).